

Theory of Sorption Hysteresis in Nanoporous Solids: I. Snap-Through Instabilities

ZDENĚK P. BAŽANT¹ AND MARTIN Z. BAZANT²

August 22, 2011

Abstract: The sorption-desorption hysteresis observed in many nanoporous solids, at vapor pressures low enough for the liquid (capillary) phase of the adsorbate to be absent, has long been vaguely attributed to changes in the nanopore structure, but no mathematically consistent explanation has been presented. The present work takes an analytical approach to account for discrete molecular forces in the nanopore fluid and proposes two related mechanisms that can explain the hysteresis at low vapor pressure without assuming any change in the nanopore structure. The first mechanism, presented in Part I, consists of a series of snap-through instabilities during the filling or emptying of non-uniform nanopores or nanoscale asperities. The instabilities are caused by non-uniqueness in the misfit disjoining pressures engendered by a difference between the nanopore width and an integer multiple of the thickness of a monomolecular adsorption layer. The second mechanism, presented in Part II, consists of molecular coalescence within a partially filled surface, nanopore or nanopore network. This general thermodynamic instability is driven by attractive intermolecular forces within the adsorbate and forms the basis to develop a unified theory of both mechanisms. The ultimate goals of the theory are to predict the fluid transport in nanoporous solids from microscopic first principles, and to determine the pore size distribution and internal surface area from sorption tests.

Introduction

The sorption isotherm, characterizing the isothermal dependence of the adsorbate mass content on the relative vapor pressure at thermodynamic equilibrium, is a basic characteristic of adsorbent porous solids. It is important for estimating the internal pore surface of hydrated Portland cement paste and other materials. It represents the essential input for solutions of the diffusion equation for drying and wetting of concrete, for calculations of the release of methane from coal deposits and rock masses, for the analysis of sequestration of carbon dioxide in rock formations, etc. Its measurements provide vital information for determining the internal surface of nanoporous solids [38, 2, 31, 3, 27, 47, e.g.].

An important feature sorption experiments with water, nitrogen, alcohol, methane, carbon dioxide, etc., has been a pronounced hysteresis, observed at both high and low vapor pressures and illustrated by two classical experiments in Fig. 1c,d) [38, p. 277] and [28] (see also [29, 40, 3, 27, 47, e.g.]). For adsorbates that exist at room temperature in a liquid form, e.g. water, the room temperature hysteresis at high vapor pressures near saturation has easily been explained by non-uniqueness of the surfaces of capillary menisci of liquid adsorbate in larger pores (e.g., the ‘ink-bottle’ effect [21]). However, a liquid (capillary) water can exist in the

¹ McCormick Institute Professor and W.P. Murphy Professor of Civil Engineering and Materials Science, Northwestern University, 2145 Sheridan Road, CEE/A135, Evanston, Illinois 60208; z-bazant@northwestern.edu (corresponding author).

² Associate Professor of Chemical Engineering and Mathematics, Massachusetts Institute of Technology, Cambridge MA 02139.

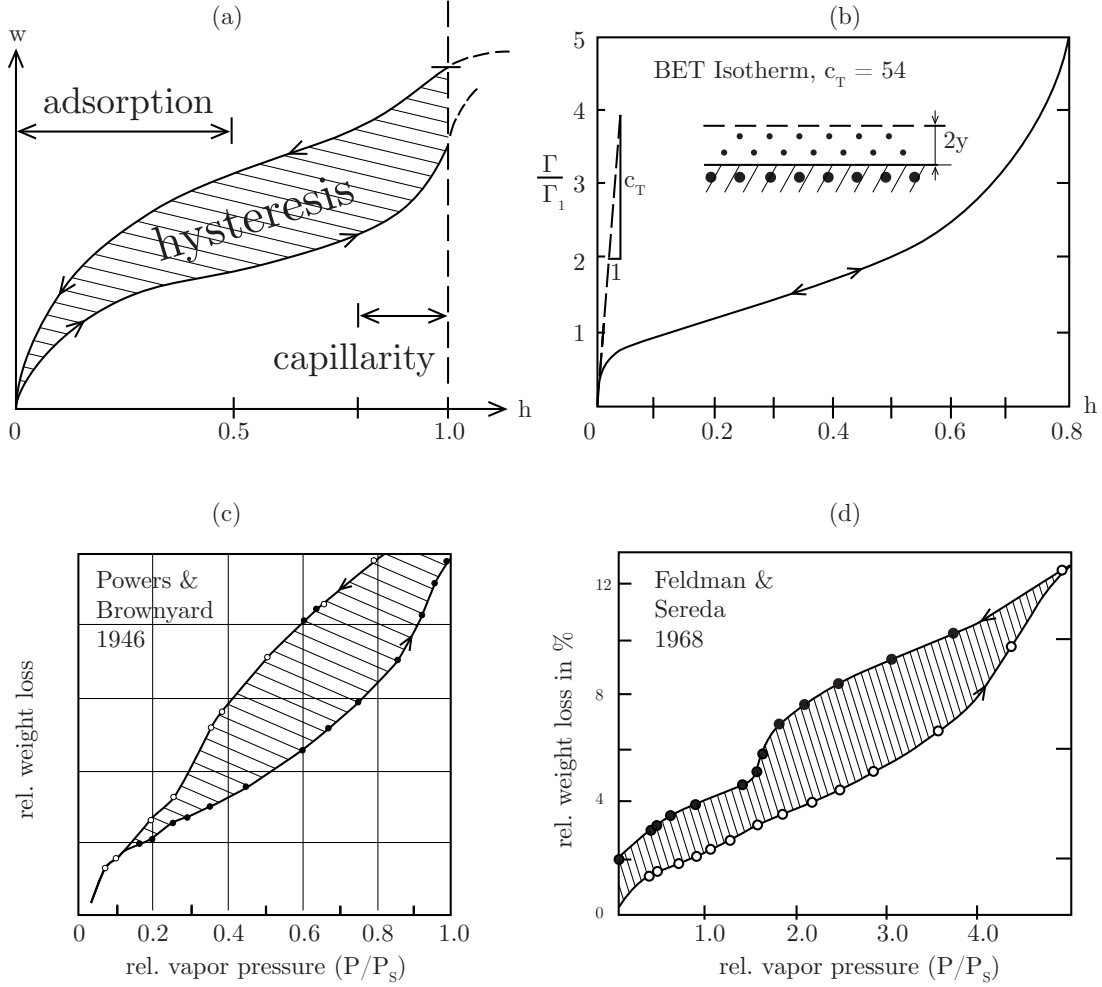


Fig. 1

Figure 1: (a) Typical desorption and sorption isotherms; (b) BET isotherm; (c)-(d) Desorption and sorption isotherms measured on hardened Portland cement paste.

pores only if the capillary tension under the meniscus (which is given by the Kelvin-Laplace equation) does not exceed the tensile strength of liquid water, which is often thought to be exhausted at no less than 45% of the saturation pressure, if not much higher. Anyway, at vapor pressures less than about 80% of the saturation pressure, the liquid phase represents a small fraction of the total evaporable water content of calcium silicate hydrates (C-S-H) [32, Fig. 3]

However, the hysteresis at low vapor pressures (lower than 80% of saturation in the case of C-S-H) has remained a perplexing and unexplained feature for over 60 years. In that case, most or all of the adsorbate is held by surface adsorption. The gases and porous solids of interest generally form adsorption layers consisting of several monomolecular layers (Fig. 1b). The multi-layer adsorption is described by BET isotherm [22] (Fig. 1a), which is reversible. Sorption experiments have generally been interpreted under the (tacit) hypothesis of free adsorption, i.e., the adsorption in which the surface of the adsorption layer is exposed to gas.

In nanoporous solids, though, most of the adsorbate is in the form of hindered adsorption

layers, i.e., layers confined in the nanopores (which are sometimes defined as pores $\leq 2\text{nm}$ wide [4]). These layers have no surface directly exposed to vapor and communicate with the vapor in macropores by diffusion along the layer. It has been well known that a large transverse stress, called the disjoining pressure [26] (or solvation pressure [4]), must develop in these layers.

Development of the theory of hindered adsorption for concrete was stimulated by Powers' general ideas on the of creep mechanism [39]. Its mathematical formulation for C-S-H gradually emerged in [5, 6, 8, 7] and was reviewed in a broad context in [9]. But this theory of hindered adsorption is also reversible. Thus, although a theory exists, it cannot explain the hysteresis.

The sorption hysteresis in hardened Portland cement paste, concrete and various solid gels [41, 33] has for a long time been vaguely attributed to some sort of changes of the nanopore structure. In particular, it was proposed that the exit or ingress of water, called the interlayer water, from or into the narrowest nanopores would somehow cause large relative changes of pore widths ([29]; see also [43], Figs. 13 and 16 in [40], Fig. 1 in [27], or Fig. 9 in [32]), picturing pore width changes $> 100\%$. However, if a mathematical model of such a mechanism were attempted it would inevitably predict enormous macroscopic deformations, far larger than the observed shrinkage caused by drying. Here it will be shown that sorption hysteresis must occur even if the nanopore structure does not change.

The salient feature of capillarity is its non-uniqueness, and the main message of this work is that an analogous non-uniqueness also applies to hindered adsorption in nanopores. In the capillary range, the non-uniqueness is classically explained by the afore-mentioned ‘‘ink-bottle’’ effect, which exists even in two dimensions. In three dimensions, there is much broader range of topological and geometrical configurations which provide a much richer and more potent source on non-uniqueness of liquid adsorbate content.

The simplest demonstration is a regular cubic array of identical spherical particles separated by a small gap δ between each pair. At $h = 1$, either all of the pore space can be filled by liquid, or an anticyclic (hyperbolic paraboloid) meniscus surface of zero total curvature $r^{-1} = r_1^{-1} + r_2^{-1} = 0$ and liquid pressure equal to p_s can exist between each two spheres, with $r_1 = -r_2$ (where $r_1, r_2 =$ principal curvature radii). This can explain 100% differences among equilibrium liquid contents w at $h = 1$ observed in some experiments. It can even be shown that when both δ and r_1 (with $r_2 = -r_1$) approach zero in a certain way, then also the liquid content (as a continuum) approaches 0. Thus, in theory, an arbitrarily small but nonzero equilibrium liquid content at $h = 1$ is possible, though extremely unlikely.

This three-dimensional picture, for example, explains why (as shown in Fig. 1a by dashed lines) the non-uniqueness of sorption isotherm extends to $h > 1$ (where $h = p_v/p_s(T) =$ relative vapor pressure, or relative humidity in the case of water, $p_v =$ pressure of vapor or gas; $p_s(T) =$ saturation vapor pressure). For $h > 1$, or $p_v > p_s$, the total curvature of the menisci is changed from positive to negative, the pores contain overpressurized vapor, and the hysteresis, or non-uniqueness continues [12, 13]. This non-uniqueness and hysteresis explains why the slope of the isotherm for $h > 1$ is one, or even two, orders of magnitude higher than one would calculate if all the water were liquid for $h > 1$. (In theory, this nonuniqueness can extend up to the critical point of water). In cements these phenomena are complicated by the fact that the chemical reactions of hydration withdraw some water from the pores, and create self-desiccation bubbles. As a result, one practically never has concrete devoid of any vapor, even for $p > p_s$.

The consequence of the non-uniqueness is that the sorption isotherm is not a function of local thermodynamic variables. Instead, it is a functional of the entire previous history of adsorbate content. Here we will show that the same functional character extends to the range of hindered adsorption in nanopores, consistent with the extensive experimental data that

consistently exhibits sorption hysteresis over the entire range of relative humidities.

The recent advent of molecular dynamic (MD) simulations is advancing the knowledge of nanoporous solids and gels or colloidal systems in a profound way [37, 23, 24, 25, 34, 35, 42, 36, 46]. Particularly exciting have been the new results by Rolland Pellenq and co-workers at the Concrete Sustainability Hub in MIT led by Franz-Josef Ulm [14, 15, 16]. These researchers used numerical MD simulations to study sorption and desorption in nanopores of coal and calcium silicate hydrates. Their MD simulations [14, Fig. 3,4] demonstrated that the filling and emptying of pores 1 and 2 nm wide by water molecules exhibits marked hysteresis.

Especially revealing is the latest paper of Pellenq et al. from MIT [15]. Simulating a chain of nanopores, they computed the distributions of disjoining (or transverse) pressure and found that it can alternate between negative (compressive) and positive (tensile), depending on the difference of pore width from an integer multiple of the natural thickness of an adsorbed monomolecular layer (see Figs. 4 and 11 in [15]). This discrete aspect of disjoining pressure, which cannot be captured by continuum thermodynamics, was a crucial finding of Pellenq et al. which stimulated the mathematical formulation of snap-through instabilities in Part I of this work. Oscillations between positive and negative disjoining pressures have also been revealed by density-functional-theory simulations of colloidal fluids or gels in [4] (where the excess transverse stress is called the “solvation pressure” rather than the disjoining pressure).

This work is organized as follows. In Part I, we begin by summarizing the classical theory of multilayer adsorption on free surfaces by Brunauer, Emmett and Teller (BET) [22], which is widely used to fit experimental data, but assumes reversible adsorption without any hysteresis. We then develop a general theory of hindered adsorption in nanopores which accounts for crucial and previously neglected effects of molecular discreteness as the pore width varies. This leads us to the first general mechanism for sorption hysteresis, snap-through instability in nonuniform pores, which is the focus of this Part I.

In Part II [1], we will show that attractive forces between discrete adsorbed molecules can also lead to sorption hysteresis by molecular coalescence in arbitrary nanopore geometries, including perfectly flat surfaces and pores. This second mechanism for hysteresis is a general thermodynamic instability of the homogeneous adsorbate that leads to stable high-density and low-density phases below the critical temperature. The mathematical formulation of the second part is thus based on non-equilibrium statistical mechanics. Similar models have been developed for surface wetting by nanoscale thin films [54, 55, 56], starting with Van der Waals over a century ago [57]. Even more relevant models, accounting for nanoscale confinement, have been developed for ion intercalation in solid nanoparticles with applications to Li-ion batteries [51, 52, 53, 50]. In that setting, analogous phenomena of hysteresis [49] (in the battery voltage vs. state of charge, in the limit of zero current) and nanoparticle size dependence [48] have now been observed in experiments. These connections, which convey the remarkable generality of hysteresis in adsorption phenomena, will be developed more in the second part in the context of a statistical physics approach. Here, in the first part, we begin to build the theory using more familiar models from solid mechanics and continuum thermodynamics.

Continuum Thermodynamics of Hindered Adsorption in Nanopores

Free Adsorption: When a multi-molecular adsorption layer on a solid adsorbent surface is in contact with the gaseous phase of the adsorbate, the effective thickness a of the layer is well

described by the BET equation [22, eq. 28]:

$$\Theta = \frac{a}{s_0} = \frac{\Gamma_w}{\Gamma_1} = \frac{1}{1-h} - \frac{1}{1-h+c_T h}, \quad c_T = c_0 e^{\Delta Q_a/RT} \quad (1)$$

where T = absolute temperature; Γ_w = mass of adsorbate per unit surface area; Γ_1 = mass of one full molecular monolayer per unit area; Θ = dimensionless surface coverage; h = relative pressure of the vapor in macropores with which the adsorbed water is in thermodynamic equilibrium; R = universal gas constant ($8314 \text{ J kmole}^{-1} \text{ }^\circ\text{K}^{-1}$); c_0 = constant depending on the entropy of adsorption; ΔQ_a = latent heat of adsorption minus latent heat of liquefaction; s_0 = effective thickness of a monomolecular layer of the adsorbate; a = effective thickness of the free adsorption layer (in contact with vapor; Fig. 1b). For the typical value of $c_T = 54$, the BET isotherm is plotted in Fig. 1b, where the number of adsorbed monolayers approaches five at the saturation pressure.

Eq. 1 can be easily inverted:

$$h = h(a) = A + \sqrt{A^2 + B} \quad (2)$$

$$\text{where } A = \frac{B c_T}{2} \left(1 - \frac{s_0}{a}\right), \quad B = \frac{1}{c_T - 1} \quad (3)$$

Hindered Adsorption: Consider now a pore with planar rigid adsorbent walls parallel to coordinates x and z and a width $2y$ that is smaller than the combined width $2a$ of the free adsorption layers at the opposite walls given by Eq. (1). Then the adsorbate has no surface in contact with the vapor and full free adsorption layers are prevented from building up at opposite pore walls, i.e., the adsorption is hindered and a transverse pressure, p_d , called the disjoining pressure [26], must develop. For water in highly hydrophilic C-S-H, the adsorption layers can be up to 5 molecules thick, and so, in pores less than 10 molecules wide ($2y < 2.6 \text{ nm}$), hindered adsorption with disjoining pressure will develop at high enough h . The adsorbent communicates by diffusion of the adsorbate along the pore with the water vapor in an adjacent macropore.

In a process in which thermodynamic equilibrium is maintained, the chemical potentials μ of the vapor and its adsorbate, representing the Gibbs' free energy per unit mass, must remain equal. So, under isothermal conditions,

$$d\mu = \rho_a^{-1}(d\tilde{p}_d + 2dp_a)/3 = \rho_v^{-1}dp_v \quad (4)$$

Here ρ = mass density of the vapor and ρ_a = average mass density of the adsorbate (which probably is, in the case of water, somewhere between the mass density ρ_w of liquid water and ice). The superior \sim is attached to distinguish the disjoining pressure obtained by continuum analysis from that obtained later by discrete molecular considerations ($\tilde{p}_d = 0$ if the nanopore is not filled because the transverse pressure due to water vapor is negligible); $p_a = \pi_a/y$ = in-plane pressure in the adsorption layer averaged through the thickness of the hindered adsorption layer; it has the dimension of N/m^2 , and (in contrast to stress) is taken positive for compression; π_a = longitudinal spreading 'pressure' in the adsorption half-layer of thickness y (here the term 'pressure' is a historically rooted misnomer; its dimension is not pressure, N/m^2 , but force per unit length, N/m); π_a is superposed on the solid surface tension γ_a , which is generally larger in magnitude, and so the total surface tension, $\gamma = \gamma_s - p_a$, is actually tensile [7, Fig. 2] (thus the decrease of spreading pressure with decreasing h causes an increase of surface tension, which is one of the causes of shrinkage).

Further note that if p_d and p_a were equal, the left-hand side would be $d\mu = \rho_a^{-1}dp_d$, which is the standard form for a bulk fluid. Also, in contrast to solid mechanics, the left-hand side of

Eq. (4) cannot be written as $\epsilon_y dp_d + 2\epsilon_x dp_a$ because strains ϵ_x and ϵ_y cannot be defined (since the molecules in adsorption layers migrate and the difference between p_d and p_a is caused by the forces from solid adsorbent wall rather than by strains).

Consider now that the ideal gas equation $p_v \rho_v^{-1} = RT/M$ applies to the vapor (M = molecular weight of the adsorbate; e.g., for water $M = 18.02$ kg/kmole). Upon substitution into Eq. (4), we have the differential equation:

$$\text{for } h \leq h_f: \quad \rho_a^{-1} dp_a = (RT/M) dp_v/p_v \quad (5)$$

$$\text{for } h > h_f: \quad \rho_a^{-1} (d\tilde{p}_d + 2dp_a)/3 = (RT/M) dp_v/p_v \quad (6)$$

where h_f = value of h at which the nanopore of width $2y$ gets filled, i.e., $h_f = h(y)$ based on Eq. (2). Factors 2 and 3 do not appear for $h < h_f$ because the free adsorbed layer can expand freely in the thickness direction. Integration of Eq. (6) under the assumption of constant ρ_a yields:

$$\text{for } h \leq h_f: \quad p_a = \frac{\pi_a}{y} = \rho_a \frac{RT}{M} \ln h \quad (7)$$

$$\text{for } h > h_f: \quad \tilde{p}_d + 2(p_a - p_{af}) = 3\rho_a \frac{RT}{M} \ln \frac{h}{h_f} \quad (8)$$

where $p_{af} = p_a(h_f)$ = longitudinal pressure when the nanopore just gets filled, i.e., when $a = y$.

It is now convenient to introduce the ratio of the increments of in-plane and disjoining pressures,

$$\kappa = dp_a / d\tilde{p}_d \quad (9)$$

which we will call the disjoining ratio. If the adsorbate were a fluid, κ would equal 1. Since it is not, $\kappa \neq 1$. The role of κ is analogous to the Poisson ratio of elastic solids. A rigorous calculation of κ would require introducing (aside from surface forces) the constitutive equation relating p_a and p_d (this was done in [11], but led to a complex hypothetical model with too many unknown parameters).

We will consider κ as constant, partly for the sake of simplicity, partly because (as clarified later) κ is determined by inclined forces between the pairs of adsorbate molecules (Fig. 3b,c); κ should be constant in multi-molecular layers because the orientation distribution of these forces is probably independent of the nanopore width. Note that κ would equal 0 only if all these intermolecular forces were either in-plane or orthogonal (Fig. 3a, as in a rectangular grid).

For constant disjoining ratio κ , we may substitute $p_a = \kappa \tilde{p}_d$ in Eq. (8), and we get

$$\tilde{p}_d = \frac{\rho_a}{1 + 2\kappa} \frac{RT}{M} \ln \frac{h}{h_f} \quad (10)$$

For $\kappa = 0$, this equation coincides with equation 29 in [7] but, in view of Fig. 3, a zero κ must be an oversimplification.

According to this continuum model of hindered adsorption, which represents a minor extension of [7], the sorption isotherm of the adsorbate mass as a function of vapor pressure would have to be reversible. However, many classical and recent experiments [38, 28, 40, 27, 47, e.g.] as well as recent molecular simulations [14, 15, 16] show it is not. Two mutually related mechanisms that must cause sorption irreversibility in nanopores with fixed rigid walls will be presented, one here in Part I, and one in Part II which follows.

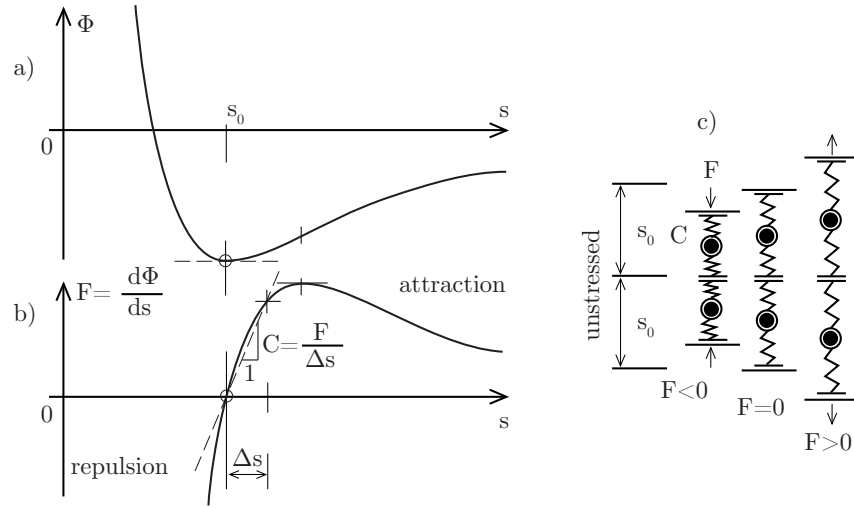


Fig. 2

Figure 2: (a) Interatomic pair potential; (b) the corresponding interatomic force and secant stiffness; (c) interatomic forces between opposite pore walls visualized by springs.

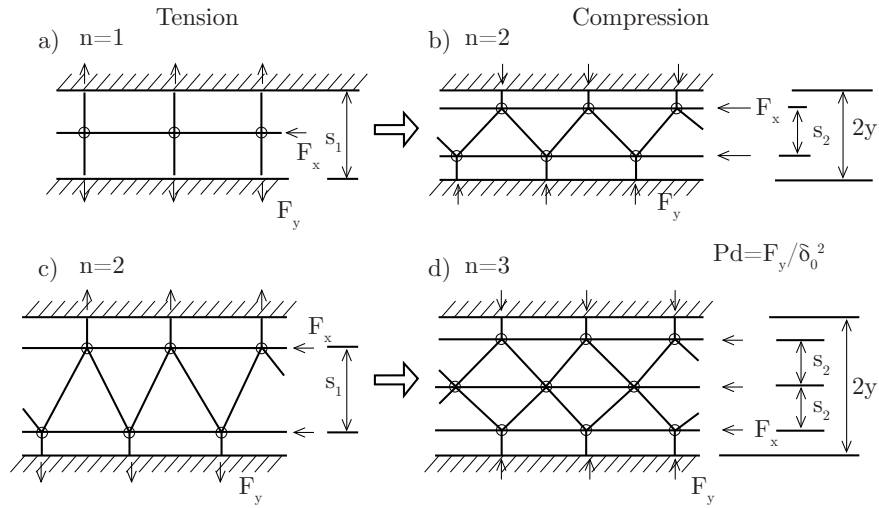


Fig. 3

Figure 3: Various simple idealized molecular arrangements between the walls of a nanopore.

Mechanism I: Snap-Through Instability

The local transverse (or disjoining) pressure p_d can be determined from the transverse stiffness C_n , defined as $C_n = \Delta F / \Delta s$ where ΔF transverse resisting force per molecule and Δs = change of spacing (or distance) between the adjacent monomolecular layers in a nanopore containing n monomolecular layers of the adsorbate. Since large changes of molecular separation are considered, C_n varies with s and should be interpreted as the secant modulus in the force-displacement diagram (Fig. 2b). For this reason, and also because many bond forces are inclined (“lateral interactions” [17, 18, 19])

rather than orthogonal with respect to the adsorption layer (shown by the bars in Fig. 3), C_n is generally not the same as the second derivative $d^2\Phi/dr^2$ of interatomic potential nor the first derivative dF/ds of force F (Fig. 2a,b).

To estimate C_n , one could consider various idealized arrangements of the adsorbate molecules (as depicted two-dimensionally for two different pore widths $2y$ in Fig. 3) and thus obtain analytical expressions for C_n based on the classical mechanics of statically indeterminate elastic trusses. However, in view of all the approximations and idealizations it makes no sense to delve into these details.

Diverging Nanopore: Consider now a wedge-shaped nanopore between two diverging planar walls of the adsorbent (Fig. 4a), having the width of $2y$ where $y = kx$. Here x = longitudinal coordinate (Fig. 4), k = constant (wedge inclination) and s_0 = effective spacing of adsorbate molecules at no stress. In the third dimension, the width is considered to be also s_0 . The adsorbate molecules are mobile and at the wide end (or mouth) of the pore they communicate with an atmosphere of relative vapor pressure h in the macropores.

We assume the hindered adsorbed layer to be in thermodynamic equilibrium with the vapor in an adjacent macropore. This requires equality of the chemical potentials $\bar{\mu}$ *per molecule* ($\bar{\mu} = \mu/M$, the overbar being used to label a quantity per molecule). At the front of the portion of the nanopore filled by adsorbate, henceforth called the ‘filling front’ (marked by circled 2, 3 or 4 in Fig. 4), Eq. (10) of continuum thermodynamics gives a zero transverse pressure, $\tilde{p}_d = 0$, and so $\bar{\mu} = \bar{\mu}_a = \bar{\mu}_v$.

However, in the discrete treatment of individual molecules, the chemical potential can be altered by transverse tension or compression Δp_d (Fig. 4), which can develop at the filling front and act across the monomolecular layers unless the nanopore width $2y$ at the filling front happens to be an integer multiple of the unstrained molecular spacing s_0 . We will call Δp_d the ‘misfit’ (part of) disjoining (or transverse) pressure, by analogy with the misfit strain energy for a dislocation core in the Peierls-Nabarro model [20].

The misfit pressure, which, at the filling front, represents the total transverse pressure (or stress), is determined by the average change Δs of spacing s between adjacent monomolecular layers, which is

$$\Delta s = 2kx/n - s_0 \quad (n = 1, 2, 3\ldots) \quad (11)$$

where n is the number of monomolecular layers across the nanopore width, and s_0 is the natural spacing between the adjacent monomolecular layers in free adsorption, i.e., when the transverse stress vanishes (note that for the triangular arrangements in Fig. 2b,c, s_0 is obviously less than the natural spacing of unstressed adsorbate molecules, shown as s_0 in Fig. 2a). So, the force between the molecules of the adjacent layers is $F = C\Delta s$ and the strain energy of the imagined springs connecting the molecules is $F\Delta s/2$ or $C(\Delta s)^2/2$ per molecule (if, for simplicity, a loading along the secant is considered).

The hindered adsorbed layer is in a multiaxial stress state, for which the total strain energy

is the sum of the strain energies of the strain components. Since continuum thermodynamics gives zero disjoining (transverse) pressure p_d at the filling front, it suffices to add to $C_n(\Delta s)^2/2$ the chemical potential $\bar{\mu}_a$ per molecule at the filling front due to longitudinal pressure p_a only. So, in view of Eq. (10), the chemical potential per molecule at the filling front x_n^f with n monomolecular layers is

$$\bar{\mu}_{f,n} = \frac{C_n}{2} \left(\frac{2kx_f}{n} - s_0 \right)^2 + \bar{\mu}_a \quad (12)$$

where the overbar is a label for the quantities per molecule. Since $\tilde{p}_d = 0$ at the filling front x^* , the only source of $\bar{\mu}_n$ is the longitudinal spreading pressure p_a in the adsorption layer.

Let us now check whether at some filling front coordinate x^* (Fig. 4) the diverging nanopore is able to contain either n or $n + 1$ monomolecular layers with the same chemical potential per molecule. For $n + 1$ layers,

$$\bar{\mu}_{f,n+1} = \frac{C_n}{2} \left(\frac{2kx}{n+1} - s_0 \right)^2 + \bar{\mu}_a \quad (13)$$

Setting $\bar{\mu}_n = \bar{\mu}_{n+1}$, we may solve for x . This yields the critical coordinate and critical pore width for which the molecules in n and $n + 1$ monomolecular layers have the same chemical potential per molecule:

$$x_{f,n}^* = \frac{\sqrt{C_n} + \sqrt{C_{n+1}}}{\frac{1}{n}\sqrt{C_n} + \frac{1}{n+1}\sqrt{C_{n+1}}} \frac{s_0}{2k}, \quad y_{f,n}^* = 2kx_{f,n}^* \quad (14)$$

So the critical relative pore width $2y_f^*/s_0$ at the filling front is a weighted harmonic mean of n and $n + 1$ (and a simple harmonic mean if $C_n = C_{n+1}$).

Equality of the chemical potentials per molecule at the filling front for n and $n+1$ monomolecular layers in the same nanopore, which occurs for the pore width given by Eq. (14), implies that no energy needs to be supplied and none to be withdrawn when the number of monomolecular layers is changed between n and $n + 1$. So the equilibrium content of hindered adsorbate in the nanopore for a given chemical potential of vapor is non-unique. Similar to non-uniqueness of capillary surfaces, this non-uniqueness underlies the sorption-desorption hysteresis in the nanopores.

Misfit Disjoining Pressure: In view of Eq. (12), its value corresponding to $\bar{\mu}_n$ for n monomolecular layers in the nanopore is

$$p_{d,n} = C_n \left(s_0 - \frac{2kx^*}{n} \right) + \tilde{p}_d(x_n) \quad (15)$$

where $\tilde{p}_d(x_n)$, based on continuum thermodynamics, is non-zero if $x_n \neq x_{f,n}$. In contrast to stress, the pressure is considered as positive when compressive. Replacing n with $n + 1$, we find that the disjoining pressure makes a jump when the number of monomolecular layers in the nanopore changes from n to $n + 1$;

$$\Delta p_{d,n} = p_{d,n+1} - p_{d,n} = 2kx_n \left(\frac{C_n}{n} - \frac{C_{n+1}}{n+1} \right) + s_0 (C_{n+1} - C_n) \quad (16)$$

(see Fig. 4). At the filling front, the jump is from transverse tension to compression (Fig. 5c). The sudden jumps $\Delta p_{d,n}$ of the misfit pressures from tension to compression diminish with

increasing n ($n = 1, 2, 3, \dots$) as the wedge-shaped nanopore is getting wider; see Figs. 5c and 4d. For $n > 10$, these jumps become insignificant.

Note that, since the changes Δs of molecular distance are large, the C values depend on F or Δp_d (Fig. 2b). So Eq. 16 is actually a nonlinear equation for Δp_d and its numerical solution would require iterations. But here we are aiming at conceptual explanation rather than numerical results.

Misfit Chemical Potentials and Their Effect on Sorption Isotherm: The variation of chemical potential at the filling front x_f is shown in Fig. 5d. Since transverse tension at the filling front gives the same chemical potential as transverse compression of equal magnitude, the misfit chemical potential, defined as the part of chemical potential due to p_d at the filling front, varies continuously, provided the pore width varies continuously, too; see Fig. 5d. This is because transverse tension gives the same chemical potential as transverse compression of equal magnitude.

The total chemical potential at the filling front is obtained by adding the chemical potential $\bar{\mu}_a(x_f)$ obtained from continuum thermodynamics, which yields the potential variation in Fig. 5e. Considering the relation of filling front coordinate x_f to the adsorbate mass w shown (in a smoothed form) in Fig. 5b, and the relation $h = e^{(M/RT)\mu_f}$, one can deduce the solid curve in Fig. 5e representing the diagram of equilibrium states of mass content w versus relative vapor pressure h in the macropore.

Why are the segments of the pressure variation in Fig. 5c linear, and why are the segments of the chemical potential variation in Fig. 5d,e,f parabolic? The reason is that the variation of nanopore width has been idealized as linear (and that the plots are made for constant C). These segments take different shapes for other width variations.

Sequential Snap-Throughs of Adsorbate Content: In sorption testing and most practical problems, the relative vapor pressure h is the variable that is controlled, and the adsorbate mass w is the response. Consequently, the states at the reversal points 1, 3, 5, 7 of the equilibrium diagram in Fig. 5 for the diverging nanopore are unstable. Likewise the states at points 1, 3, 5, 7 in Fig. 6d for the nanopore of step-wise variable width. The loss of stability can be evidenced by checking that the molecular potential loses positive definiteness. Fundamental though such checks may be, it is simpler and more intuitive to argue in terms of infinitely small deviations dh from the equilibrium state.

Consider, e.g., that, in Fig. 5f or 6d, a sufficiently slow gradual increase of h has moved the equilibrium state from point 2 to point 3, which is a local maximum of h as a function of w . For a further infinitesimal increase dh there is on the equilibrium diagram no longer any point close to point 3. So, borrowing a term from structural mechanics [10], we realize that the adsorbate mass content w must dynamically ‘snap through’ at constant h along vertical line 34 to point 4. After dissipating the energy released along segment 34 (the rate of which depends on the lingering times of adsorbed molecules and diffusion along the hindered adsorbed layer [11]), thermodynamic equilibrium is recovered at point 4. It is stable because a further infinitesimal increment of dh finds, next to point 4, an equilibrium state with adsorbate content incremented by dw .

If h is increased slowly enough further, the equilibrium system will move from point 4 to point 5 at which a local maximum of h is reached again and the loss of stability gets repeated, since a further increase dh can find equilibrium only after a dynamic snap-through to point 6. Each snap-through will release some energy which must be damped and dissipated by the system. So the local maxima of h at points 1, 3, 5 and 7 are the critical states giving rise to the so-called ‘snap-through instability’ [10]. The equilibrium states on curved segments 1e2,

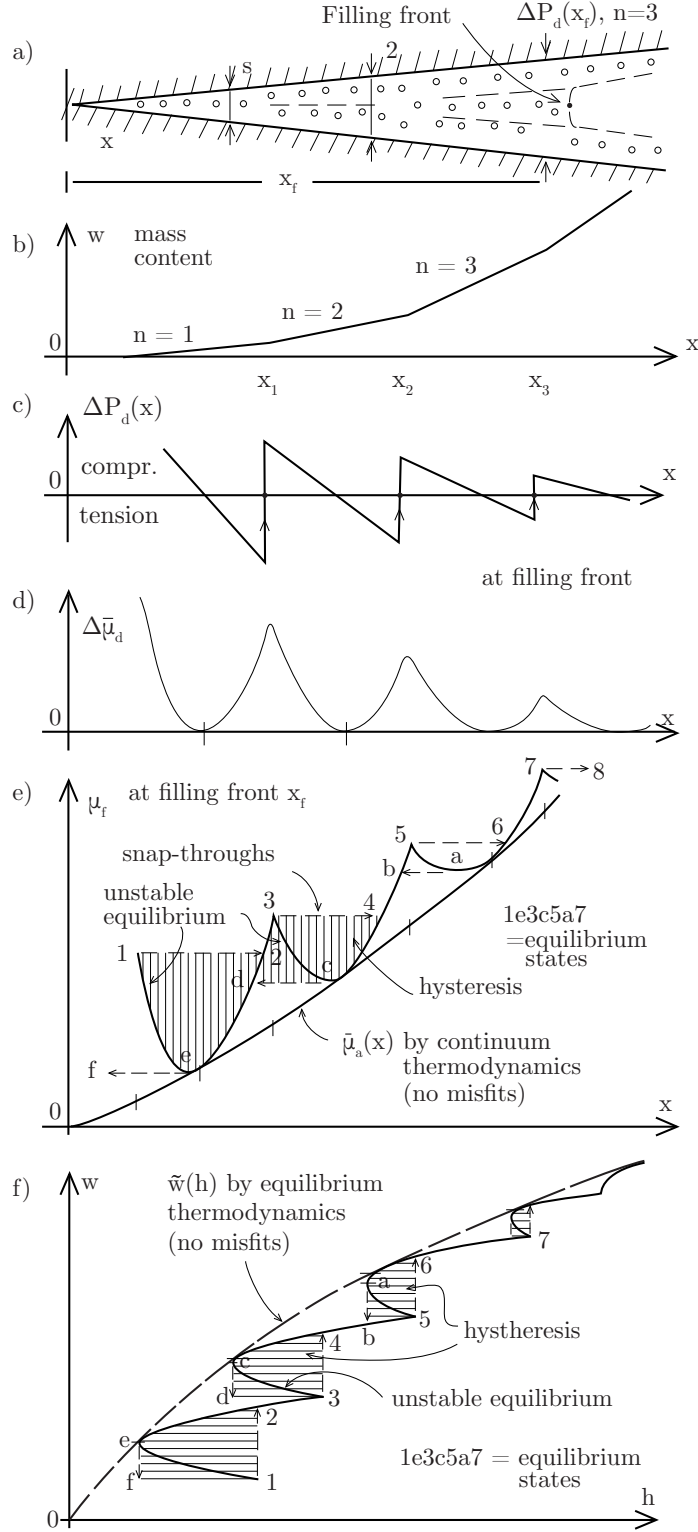


Fig. 5

Figure 5: Misfit disjoining pressures and chemical potentials in a continuously diverging nanopore, with dynamic snap-throughs of adsorbate content.

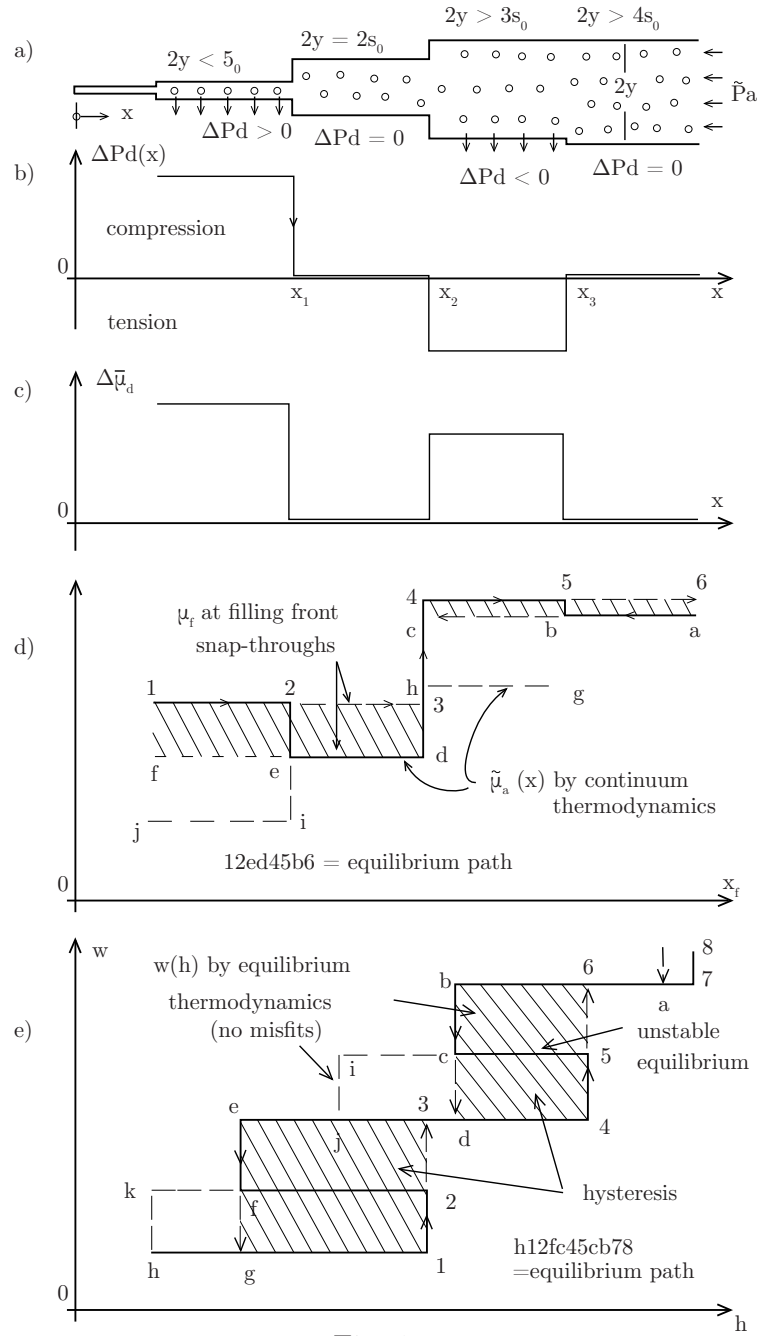


Fig. 6

Figure 6: Step-wise diverging nanopore and misfit disjoining pressures.

3c4 and 5a6 are unstable and can never be reached in reality.

The salient feature is that a different path $w(h)$ is followed when h is decreased. To show it, consider point 7 in Fig. 5f or 6d as the starting point. During a slow enough decrease h , the system will follow the stable states along segment 76a until a local minimum of h is reached at point a , which is the stability limit. Indeed, if h is further decremented by dh , there is no equilibrium state near point a . So the equilibrium state a is unstable and the system will ‘snap through’ dynamically at constant h along path ab . At point b stable equilibrium is regained after sufficient time. When h is decreased further slowly enough, the equilibrium states move through segment b4c until again a local minimum of h is reached and stability is lost at point c . Thereafter, the system ‘snaps through’ along line cd to point d , where equilibrium is regained, etc.

In the diverging pore in Fig. 5, the snap-through means that when the equilibrium filling front reaches the critical points, x_1, x_2 , or x_3 , it will advance forward a certain distance at constant h , as fast as diffusion along the micropore, controlled by the lingering times of the adsorbate molecules, will permit. The cross-hatched areas in between the sorption and desorption isotherms, such as area 34cd3 in Fig. 5e or Fig. 6d, represent sorption hysteresis. They also characterize energy dissipation.

Sequential Snap-Throughs for Step-Wise Nanopore Width Variation: The diagrams in Fig. 5d,e,f are valid only for a micropore with continuously diverging rigid planar walls (Fig. 5a). This is, of course, an idealization. Because of the atomistic structure of pore walls, the pore width in reality varies discontinuously, as exemplified in Fig. 6a. The chance of a width exactly equal to an integer multiple of s_0 is small.

Consider that the jumps of nanopore width (Fig. 6a) occur at x_1, x_2, x_3, \dots , and that at x_1 is narrower than s_0 , at x_2 exactly equal to $2s_0$, and at x_3 wider than $3s_0$. Thus the filling front in pore segment (x_1, x_2) is in transverse compression, in segment (x_2, x_3) at zero transverse pressure, and in segment (x_3, x_4) in transverse tension; see Fig. 6b. The corresponding strain energies, representing the misfit chemical potential $\Delta\bar{\mu}_d$ per molecule, have a pulse-like variation as shown in Fig. 6c. Continuum thermodynamics, which ignores the misfits, gives a monotonically rising staircase variation of the chemical potential $\bar{\mu}_a(x)$ (per unit mass) as a function of the filling front coordinate x_f , represented by path $jiedhgba$ (Fig. 6d). Superposing on this staircase the misfit chemical potential $\Delta\bar{\mu}_d$ (converted to unit mass), one gets the non-monotonic step-wise path of equilibrium states, shown by the bold line 12ed455b6 in Fig. 6d.

Taking into account the dependence of the adsorbate mass w in the nanopore on the filling front coordinate x_f , one can convert the diagram in Fig. 6d into the sorption isotherm in Fig. 6e, usually plotted as w versus h . The monotonic staircase $hkfejicba$ would represent the equilibrium path if the misfit disjoining pressures were ignored.

When the rise of h , and thus μ_f , is controlled, the segments 23 and 56 in Fig. 6e are unstable and unreachable. Indeed, when h or μ_f is infinitesimally increased above point 2, there is no nearby equilibrium state, and so the system will ‘snap through’ dynamically to point 3. At that point, equilibrium is regained, and h and μ_f can be raised again, slowly enough to maintain equilibrium, along path 345. A similar dynamic snap-through is repeated along segment 56, after which the stable segment 678 can be followed. Likewise, in the diagram of μ_f versus the filling front coordinate x_f (Fig. 6d), forward snap-throughs at increasing μ_f (which is a monotonically increasing function of h) occur along segments 23 and 56.

When h or μ_f is decreased slowly enough from point 8, the stable equilibrium path 876bc is followed until stability is lost at point c (Fig. 6e). Then the system snaps through dynamically

from c to d , follows equilibrium path def , and snaps dynamically from f to g . Likewise, in Fig. 6d, backward snap-throughs at decreasing μ_f occur along segments bc and ef .

Obviously, the states on segments $c5$ and $f2$ in Fig. 6e, or $2e$ and $5e$ in Fig. 6d, can never be reached. They represent unstable equilibrium. The shaded areas $g13eg$ and $d46bd$ represent hysteresis, which leads to energy dissipation.

Snap-Throughs in a System of Nanopores: The diverging nanopore (Fig. 4, 5a and 6a) is not the only pore geometry producing sorption hysteresis. There are infinitely many such geometries. In the simple model of discrete monolayers pursued in Part I, the only geometry avoiding hysteresis due to sequential snap-throughs is hypothetical—the widths of all the nanopores would have to be exactly equal to the integer multiples of the natural spacing s_0 of monomolecular layers in free adsorption, so as to annul the misfit pressures. Below, we will show that if molecular coalescence is allowed in the lateral direction, then even these special pore geometries will exhibit sorption hysteresis, and so the effect is extremely general.

An essential feature of nanoporosity is that there are nanopores of many different thicknesses $2y$ densely distributed as shown in Fig. 7. At a given vapor pressure, all the nanopores that are narrower than a certain width $2y$ are filled by adsorbed water and the wider ones are empty, containing only vapor; see Fig. 7a,c,e.

As the relative pore pressure h is increased, larger and larger pores fill up. A critical state (or a local maximum of h) is reached for a pore width at which the misfit chemical potential $\Delta\mu_d$ due to misfit disjoining pressure is for n monomolecular layers equal to or larger than the misfit chemical potential for $n+1$ layers. After that state, the system loses stability and regains it only when all the nanopores up to a certain larger width get filled without increasing h . For decreasing h , the stability loss would occur for a different pore width.

The distribution of nanopore thicknesses $2y$ may be characterized by a continuous cumulative frequency distribution function $\varphi(y)$ that represents the combined volume of all the nanopores with thicknesses $< 2y$. This case, though, is not qualitatively different from the diverging nanopore studied previously. For $\varphi(y) \propto ky^2$, the nanopore system in Fig. 7 becomes mathematically equivalent to the linearly diverging nanopore studied before.

The way the hysteresis in the individual nanopores gets superposed to produce a pronounced hysteresis on the macroscale is schematically illustrated in Fig. 8.

Analogy with Snap-Through Buckling of Flat Arch: There is an instructive analogy with the snap-through buckling of elastic arches or shells under controlled load (Fig. 9 [10, p.231]. If the arch is flat enough and flexible enough not to fracture, the equilibrium diagram of total load p versus midspan deflection u follows the diagram sketched in Fig. 9. The segments 051 and 432 consist of stable states at which the potential energy is positive definite (i.e., has a strict local minimum). But this is not true for the equilibrium states on the segment 12, at which the potential energy does not have a strict local minimum.

Consider that load p is increased from point 0 up to the local maximum at critical point 1 (Fig. 9). If load p is increased further by an infinitesimal amount ddp , there is no nearby equilibrium state. The arch must follow at constant load the dynamic snap-through path 14, during which there is accelerated motion, with the load difference from the equilibrium curve below being equal to the inertial force, which provides rightward acceleration. The arch gains kinetic energy up to point 3, swings over (along a horizontal line), and then vibrates at constant load about point 3 until the kinetic energy is dissipated by damping (without damping, it would vibrate indefinitely). Then, if the load is increased further, the arch moves through stable equilibrium states on the segment 34.

When the load is decreased, starting at point 4, the arch will follow the stable equilibrium

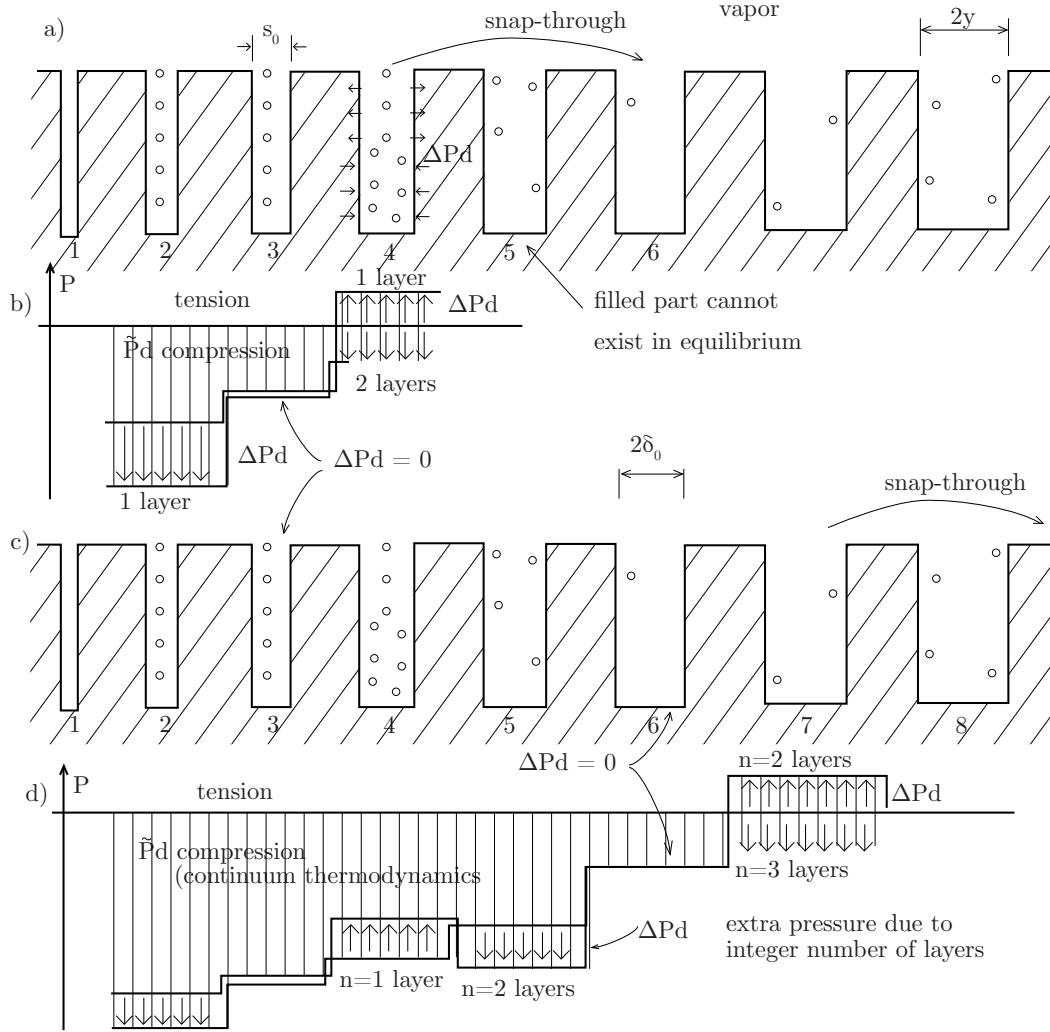


Fig. 7

Figure 7: System of nanopores of different widths communicating through vapor phase .

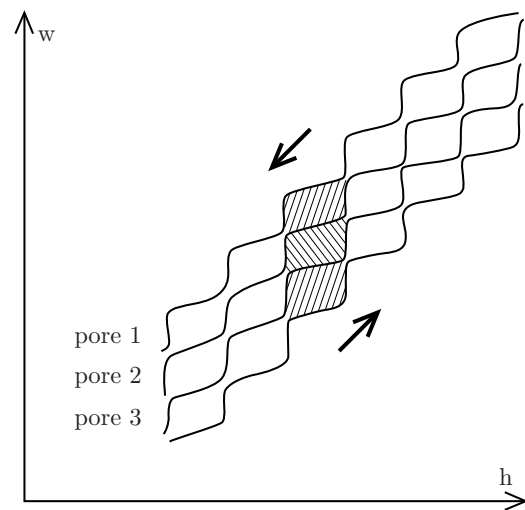


Fig. 8

Figure 8: Superposition of hysteretic loops from different nanopores.

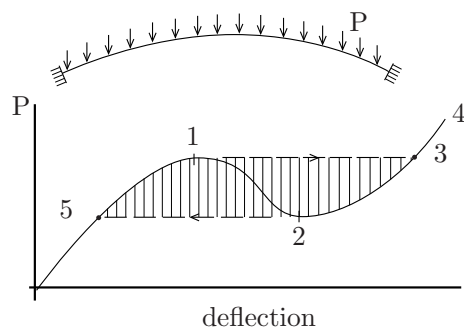


Fig. 9

Figure 9: Analogy with snap-through of an arch.

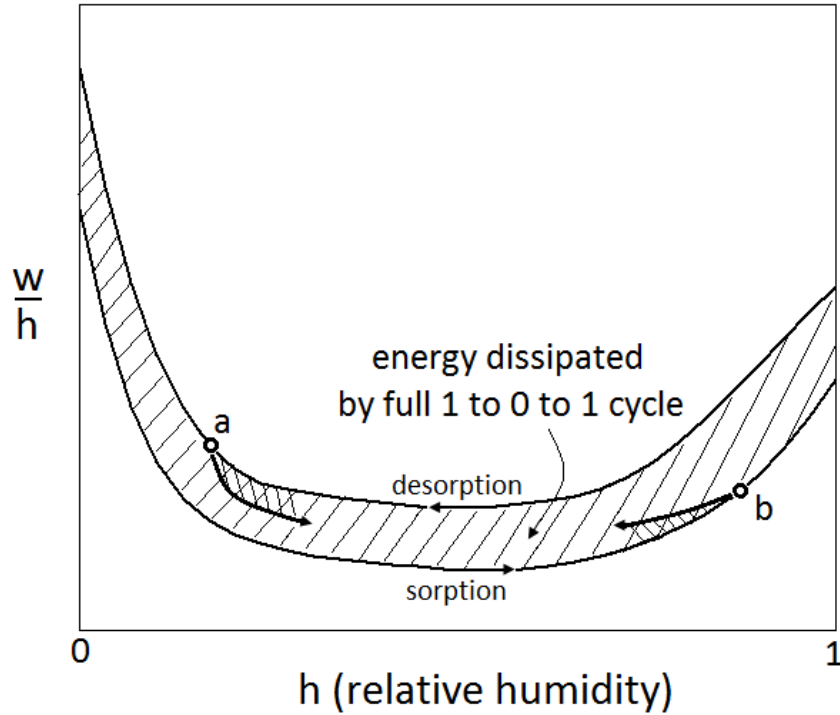


Figure 10: Energy dissipated by sorption hysteresis on a full h -cycle $1 \rightarrow 0 \rightarrow 1$ (shaded area), and dissipation during mid-range reversals (a,b).

states along segment 432 until a local minimum is reached at point 2. If the load is decreased further by an infinitesimal amount dP , there is no equilibrium state near point 2. So the arch must snap through dynamically to point 5, the load being again balanced by inertia forces which provide leftward acceleration. During this snap-through the arch gains kinetic energy, swings over to the left of point 5 and vibrates about point 5 until the kinetic energy is dissipated by damping. Then the load can be decreased further following the stable equilibrium states below point 5.

Note that even though the arch is elastic and the structure-load system is conservative, hysteresis is inevitable. During the cycle, the arch dissipates an energy equal to the cross-hatched area 51325 in Fig. 4.

Energy Dissipated by Hysteresis and Material Damage: The Gibbs free energy dissipated per unit mass of the nanoporous material is $dG = w d\mu$ where $d\mu = \frac{RT}{M} d \ln h$, which has in thermodynamic equilibrium the value for the adsorbate species in the vapor and for the adsorbed phases. Therefore, the free energy dissipated per unit volume of material due to the hysteresis during a complete cycle, e.g., a drying-wetting cycle of hardened cement paste, is

$$\Delta G = \frac{RT}{M} \oint \frac{w(h)}{h} dh \quad (17)$$

Since h is in the denominator, integrability, i.e., the finiteness of ΔG , requires that $\lim_{h \rightarrow 0} w/h = 1/h^n$ where $0 \leq n < 1$. Graphically, ΔG is proportional to the area between the sorption and desorption isotherms in the diagram of w/h versus h (Fig. 10).

The energy could be dissipated in two ways:

- 1) By internal friction in the adsorbed fluid during the dynamic snap-throughs (or the

molecular coalescence phenomena discussed in Part II [1]), or

2) by fracturing or plastic damage to the nanopore surfaces.

However, the latter seems unlikely since it could be associated with every disjoining pressure change and not particularly with the snap-through. The existence of the former is undeniable, and the point here is to show that the hysteresis is perfectly explicable without postulating any damage to the nanopore surface.

Anyway, the degree of material damage due to a drying-wetting cycle, if any, could be checked by measuring the strength or the fracture energy, or both, of the material before and after the cycle. This would have to be done slowly enough on thin enough specimens having drying half-times less than 1 hour (< 1 mm thick for cement paste), in which the relative humidity h in the capillary pores can be changed without creating a significant gradient of h across the specimen wall (in thicker samples, most of the material damage is done by non-uniform shrinkage stresses engendered by non-uniformity of h across the wall thickness [45]). Shrinkage and creep experiments on such specimens have been performed at Northwestern [44], but no cycles were performed and strength changes were not checked. It could also be checked whether the snap-throughs might be associated with the acceleration of concrete creep due to simultaneous drying, called the drying creep (or Pickett effect).

Sorption Potential: Note that, based on the derivation of Eq. (17), it further follows that

$$\beta = \frac{RT}{M} \frac{w}{h} = \frac{\partial G}{\partial h} \quad (18)$$

In other words, the Gibbs's free energy per unit mass of adsorbate as a function of h is a potential for the adsorbate content parameter β during a one-way change of h .

Conclusions of Part I

We can summarize the findings of the first part as follows:

1. One mechanism that must be causing sorption hysteresis at low vapor pressure is a series of snap-through instabilities causing path-dependent non-uniqueness of adsorbate content and dynamic jumps of water content of nanopores at constant vapor pressure.
2. The snap-through instabilities are a consequence of the discreteness of the adsorbate, which leads to non-uniqueness of mass content and to misfit disjoining (transverse) pressures due to a difference between the pore width and an integer multiple of the thickness of a transversely unstressed monomolecular layer of the adsorbate.
3. The hysteresis is explained by the fact that the snap-through instabilities for sorption and desorption follow different paths.
4. The snap-through instabilities are analogous to snap-through buckling of arches and shells, long known in structural mechanics. They cause hysteresis and energy dissipation even when the arch or shell is perfectly elastic.

If a quantitative version of this theory were developed, it might be possible to infer from the hysteresis the surface area and the size distribution of the nanopores filled by hindered adsorbate. Our preliminary analysis of snap-through instabilities suggests that the key to making this connection is to account for inclined forces, or "lateral interactions", in the statistical thermodynamics of hindered adsorption. In the Part II, we will show that attractive lateral interactions

generally lead to sorption hysteresis in any pore geometry due to molecular coalescence of the adsorbate.

Acknowledgment: The research was funded partly by the U.S. National Science Foundation under Grant CMS-0556323 to Northwestern University (ZPB) and Grant DMS-0948071 to MIT (MZB) and partly by the U.S. Department of Transportation under Grant 27323 provided through the Infrastructure Technology Institute of Northwestern University (ZPB). Thanks are due to Franz-Josef Ulm and Rolland J.-M. Pellenq of MIT for stimulating discussions of disjoining pressure based on MD simulations, and to Laurent Brochard and Hamlin M. Jennings for further valuable discourse.

References

- [1] Bazant, M. Z. and Bažant, Z. P. “Theory of sorption hysteresis in nanoporous solids: II. Molecular coalescence”. preprint.
- [2] Adolphs, J., and Setzer, M.J. (1996). “A model to describe adsorption isotherms.” *J. of Colloid and Interface Science* 180, 70–76.
- [3] Adolphs, J., Setzer, M.J. and Heine, P. (2002). “Changes in pore structure and mercury contact angle of hardened cement paste depending on relative humidity.” *Materials and Structures* 35, 477–486.
- [4] Balbuena, P.B., Berry, D., and Gubbins, K.E. (1993). “Solvation pressures for simple fluids in micropores.” *J. Phys. Chem.* 97, 937–943.
- [5] Bažant, Z.P. (1970). “Constitutive equation for concrete creep and shrinkage based on thermodynamics of multi-phase systems.” *Materials and Structures*, 3, 3–36 (reprinted in *Fifty Years of Evolution of Science and Technology of Building Materials and Structures*, Ed. by F.H. Wittmann, RILEM, Aedificatio Publishers, Freiburg, Germany 1997, 377–410).
- [6] Bažant, Z.P. (1970). “Delayed thermal dilatations of cement paste and concrete due to mass transport.” *Nuclear Engineering & Design*, 24, 308–318.
- [7] Bažant, Z.P. (1972). “Thermodynamics of interacting continua with surfaces and creep analysis of concrete structures.” *Nuclear Engineering and Design*, 20, 477–505.
- [8] Bažant, Z.P. (1972). “Thermodynamics of hindered adsorption with application to cement paste and concrete.” *Cement and Concrete Research*, 2, 1–16.
- [9] Bažant, Z.P. (1975). “Theory of creep and shrinkage in concrete structures: A précis of recent developments”, *Mechanics Today*, ed. by S. Nemat-Nasser (Am. Acad. Mech.), Pergamon Press 1975, Vol. 2, pp. 1–93.
- [10] Bažant, Z.P., and Cedolin, L. (1991). *Stability of Structures: Elastic, Inelastic, Fracture and Damage Theories*, Oxford University Press, New York; 2nd. ed. Dover Publ. 2003; 3rd ed. World Scientific Publishing, Singapore–New Jersey–London 2010.
- [11] Bažant, Z.P., and Moschovidis, Z. (1973). “Surface diffusion theory for the drying creep effect in Portland cement paste and concrete” *J. Am. Ceramic Soc.*, 56, 235–241.
- [12] Bažant, Z.P., and Thonguthai, W. (1978). “Pore pressure and drying of concrete at high temperature.” *Proc. ASCE, J. of the Engrg. Mech. Div.*, 104, 1058–1080.
- [13] Bažant, Z.P., and Kaplan, M.F. (1996). *Concrete at High Temperatures: Material Properties and Mathematical Models*, Longman (Addison-Wesley), London; 2nd ed. Pearson Education, Edinburgh, 2002.
- [14] Bonnaud, P.A., Coasne, B., and Pellenq, R.J.-M. (2010). “Molecular simulation of water confined in nanoporous silica.” *J. Phys.: Condens. Matter*, 284110 (15pp).
- [15] Brochard, L., Vandamme, M. and Pellenq, R.J.-M. (2011). Competitive adsorption of carbon dioxide and methane in coal.” Privately communicated manuscript, submitted to PNAS.
- [16] Brochard, L., Vandamme, M. and Pellenq, R.J.-M. (2011). Poromechanics of nanoporous media.” Privately communicated manuscript; submitted to *J. of the Mech. and Phys. of Solids*.

- [17] Nikitas, P. (1996). "A simple statistical mechanical approach for studying multilayer adsorption: Extensions of the BET adsorption isotherm." *J. Phys. Chem.* 100, 15247–15254.
- [18] Cerofolini, G.F., Meda, L. (1998). "A theory of multilayer adsorption on rough surfaces in terms of clustering and melting BET piles." *Surface Science* 416, 402–432.
- [19] Cerofolini, G.F., Meda, L. (1998). "Clustering and melting in multilayer equilibrium adsorption." *J. of Colloid and Interface Science* 202, 104–123.
- [20] Hirth, J. P. and Lothe, J., *Theory of Dislocations*, (Kreiger, 1992).
- [21] Brunauer, S. (1943). *The adsorption of gases and vapors*. Princeton University Press, Princeton, NJ, 1943 (p. 398).
- [22] Brunauer, S., Emmett, P.T., and Teller, E. (1838). "Adsorption of gases in multi-molecular layers." *J. Amer. Chemical Soc.* 60, 309–319.
- [23] B. Coasne, A. Galarneau, F. Di Renzo, and R. J.-M. Pellenq (2009). "Intrusion and retraction of fluids in nanopores: effect of morphological heterogeneity", *J. Phys. Chem. C* 113, 1953–1962.
- [24] B. Coasne, A. Galarneau, F. Di Renzo, and R. J.-M. Pellenq (2008). "Molecular simulation of adsorption and intrusion in nanopores." *Adsorption* (2008) 14: 215–221.
- [25] B. Coasne, F. Di Renzo, A. Galarneau and R.J.-M. Pellenq (2008). "Adsorption of simple fluid on silica surface and nanopore: effect of surface chemistry and pore shape." *Langmuir* 24, 7285–7293
- [26] Derjaguin, B.V. (1940). "On the repulsive forces between charged colloid particles and the theory of slow coagulation and stability of lyophole sols, *Trans. of the Faraday Society* 36, 203, 730.
- [27] Espinosa, R.M., and Franke, L. (2006). "Influence of the age and drying process on pore structure and sorption isotherms of hardened cement paste." *Cement and Concrete Research* 36, 1969–1984 (Figs. 2, 6, 16).
- [28] Feldman, R.F., and Sereda, P.J. (1964). "Sorption of water on compacts of bottle hydrated cement. I: The sorption and length-change isotherms." *J. Appl. Chem.* 14, p.87.
- [29] Feldman, R.F., and Sereda, P.J. (1968). "A model for hydrated Portland cement paste as deduced from sorption-length change and mechanical properties." *Materials and Structures* 1 (6) (1968) 509–520.
- [30] Frenkel, D., and Smit, B. (1996). *Understanding Molecular Simulations*. Academic Press, Sand Diego–New York.
- [31] Jennings, H.M. (2000). "A model for the microstructure of calcium silicate hydrate in cement paste." *Cement and Concrete Research* 30, 101–116.
- [32] Jennings, H.M. (2010). "Pores and viscoelastic properties of cement paste." submitted to an Elsevier Science journal.
- [33] Jennings, H.M., Bullard, J.W., Thomas, J.J., Andrade, J.E., Chen, J.J., and Scherer, G.W. (2008). "Characterization and modeling of pores and surfaces in cement paste: Correlations to processing and properties." *J. of the Advanced Concrete Technology* 6 (1), 5–29.
- [34] Jönson, B., Nonat, A., Labbez, C., Cabane, B., and Wennerström, H. (2005). "Controlling the cohesion of cement paste." *Langmuir* 21, 9211–9221.
- [35] Jönson, B., Wennerström, H. Nonat, A., and Cabane, B. (2004). "Onset of cohesion in cement paste." *Langmuir* 20, 6702–6709.
- [36] Malani, A., Ayappa, K.G., and Murad, S. (2009). "Influence of hydrophilic surface specificity on the structural properties of confined water." *J. Phys. Chem.* 113, 13825–13839.
- [37] Pellenq, R. J.-M., Kushima, A., Shashavari, R., Van Vliet, K.J., Buehler, M.J., Yip, S. and Ulm, F.-J. (2010). "A realistic molecular model of cement hydrates." *Proc. Nat. Academy of Sciences* 106 (38), 16102–17107.
- [38] Powers, T.C., and T.L. Brownyard (1946), "Studies of the Physical Properties of Hardened Portland Cement Paste. Part 2. Studies of Water Fixation". *J. of the Am. Concrete Institute* 18(3), 249–336.
- [39] Powers, T.C. (1966). "Some observations on the interpretation of creep data." *Bulletin RILEM (Paris)*, p. 381.

- [40] Rarick, R.L., Bhatt, J.W. and Jennings, H.M. (1995). "Surface area measurement using gas sorption: Application to cement paste." *Material Science of Concrete IV*, edited by J. Skalny and S. Mindess, Am. Ceramic Soc., Chapter 1, pp. 1–41.
- [41] Scherer, G.W. (1999). "Structure and properties of gels." *Cement and Concrete Research* 29 (1999), 1149–1157.
- [42] Smith, D.E., Wang, Y., Chaturvedi, A., Whitley, H.D. (2006). "Molecular simulations of the pressure, temperature, and chemical potential dependencies of clay swelling." *J. Phys. Chem. B* 110, 20046–20054.
- [43] Thomas, J.J., Allen, A.J., and Jennings, H.M. (2008). "Structural changes to the calcium hydrate gel phase of hydrated cement with age, drying and resaturation." *J. of the Am. Ceramic Soc.* 91 (10), 3362–3369.
- [44] Bažant, Z.P., Asghari, A. A., and Schmidt, J. (1976). "Experimental study of creep of hardened cement paste at variable water content." *Materials and Structures* (RILEM, Paris), 9, 279–190.
- [45] Bažant, Z.P., and Raftshol, W. J. (1982). "Effect of cracking in drying and shrinkage specimens." *Cement and Concrete Research*, 12, 209–226; Disc. 797–798.
- [46] M. Vandamme, L. Brochard, B. Lecampion and O. Coussy (2010) "Adsorption and strain: The CO₂-induced swelling of coal," *J. of the Mechanics and Physics of Solids* 58, 1489-1505.
- [47] Baroghel-Bouny, V. (2007) "Water vapour sorption experiments on hardened cementitious materials Part I: Essential tool for analysis of hygral behaviour and its relation to pore structure" *Cement and Concrete Research* 37, 414437.
- [48] Wagemaker, M., Singh, D. P., Borghols, W. J. H., Lafont, U., Haverkate, L., Peterson, V. K. and Mulder, F. M. (2011) "Dynamic Solubility Limits in Nanosized Olivine LiFePO₄", *J. Am. Chem. Soc.*, 133, 1022210228.
- [49] Dreyer, W., Jamnik, J., Gohlke, C., Huth, R., Moškon, J., and Gaberšček, M. (2010). "The thermodynamic origin of hysteresis in insertion batteries." *Nature Materials* 9, 448–451.
- [50] Dreyer, D., Gohlke, C., and Huth, R. (2011) "The behavior of a many-particle electrode in a lithium-ion battery", *Physica D* 240, 10081019
- [51] G. K. Singh, G. Ceder and M. Z. Bazant (2008) "Intercalation dynamics in rechargeable battery materials: General theory and phase transformation waves in LiFePO₄," *Electrochimica Acta* 53, 7599.
- [52] D. Burch and M. Z. Bazant (2009) "Size dependent spinodal and miscibility gaps in nanoparticles," *Nano Letters* 9, 3795.
- [53] Bai, P., Cogswell, D. A., and Bazant, M. Z. (2011) "Suppression of phase separation in LiFePO₄ nanoparticles during battery discharge", preprint, arXiv:1108.2326v1 [cond-mat.mtrl-sci]
- [54] de Gennes, P. G. (1985) "Wetting: statics and dynamics", *Rev. Mod. Phys.* 57, 827-863.
- [55] Gouin H. and Gavrilyuk, S. (2008) "Dynamics of liquid nanofilms", *Int. J. Eng. Sci.* 46, 1195-1202.
- [56] Gouin H. (2009) "Liquid nanofilms: A mechanical model for the disjoining pressure ", *Int. J. Eng. Sci.* 47, 691-699.
- [57] van der Waals, J. D. (1893). The thermodynamic theory of capillarity under the hypothesis of a continuous variation of density. (Translation by J. S. Rowlinson (1979)) *Journal of Statistical Physics*, 20, 197 (Original version: *Zeitschrift fuer Physikalische Chemie, Stoechiometrie und Verwandtschaftslehre*, 13, 657).